# Application of deterministic and stochastic analysis to calculate a stadium with pressure measurements in wind tunnel

N. Blaise[1], G. Grillaud[2], V. De Ville de Goyet[3], V. Denoël[1]
[1]Department of Architecture, Geology, Environment and Construction, University of Liège, Chemin des Chevreuils, 1, Bât B 52/3, 4000 Liège , Belgium
[2] Centre Scientifique et Technique du Bâtiment (CSTB), rue Henri Picherit 11, 44323 Nantes, France
[3]Bureau d'Etudes Greisch, Allée des Noisetiers, 25, 4031 Angleur, Belgium
email: N.Blaise@ulg.ac.be, gerard.grillaud@cstb.fr, vdeville@greisch.com, V.Denoel@ulg.ac.be

ABSTRACT: This paper aims at comparing different analysis methods in the design of a roof subjected to buffeting wind forces. The specificity of this study is that aerodynamic pressures acting on the stadium roof are measured in a wind tunnel. Commonly a deterministic approach is considered in that context and modal superposition is applied. Uncoupled modal equations are solved either in the time domain with a step-by-step method, either in the frequency domain. As an alternative, we seek to apply the concepts of a stochastic analysis using the background resonant decomposition. The key idea is to fit a probabilistic model onto the measured data and to perform the stochastic analysis as a usual buffeting analysis. An important focus is put on the ultimate goal of designing the structure, i.e. of computing extreme values of representative internal forces in the structure. This is performed with dedicated approaches for deterministic and stochastic analyses.The deterministic approach is able to capture the non Gaussian nature of the loading and provides therefore positive and negative peak factors. On the contrary, in the stochastic approach limited to the second order here (Gaussian context), Rice's formula provides a unique peak factor and therefore advanced techniques need to be applied in order to provide suitable estimations of extreme values. This difficulty to model extreme values is a drawback of the stochastic approach that could be solve by reproducing at higher statistical orders the principles of the method presented in this paper. For a number of reasons explained in the paper, the stochastic approach performs better than the deterministic one.

KEY WORDS: Buffeting wind forces; Roof; Stochastic analysis; Background resonant decomposition; Extreme values; Non Gaussian; Peak factor; Wind tunnel.

## 1 INTRODUCTION

Design of structures subjected to wind loads can be performed with various analysis methods. The equation of motion may be solved with three approaches. A first option is a deterministic approach [1] with modal superposition. Uncoupled modal equations are solved either with a step-by-step method, either in the frequency domain, by Fourier transform and multiplication by the transfer function. A second possibility is a stochastic analysis [2], using background resonant decomposition (SRSS and CQC) [3]. The choice of one or another method depends on the time/frequency and deterministic/stochastic nature of the loading.

In a wind tunnel context, the loading is defined sometimes by synchronous pressure measurements, given as time history recordings. Because wind tunnel measurements inherently present some limitations (e.g. data acquisition rate), the description by means of time histories can be less appropriate to cope with at a design stage, than a more traditional buffeting loading model. These limitations make some methods more suitable than others, although the deterministic approach would appear to be the most appropriate at first glance.

The aim of this paper is to apply and compare deterministic and stochastic analyses in the design of a stadium roof subjected to wind forces. Deterministic approaches require only the measured pressures whereas the stochastic approach needs a processing of these measured signals (calculation of Power Spectral Densities, PSD, for example) to put them into a probabilistic model which is the key idea developed in this paper. Some limitations at the deterministic method are pointed up and explained. After, the evaluation of the extreme values and their non Gaussian nature is discussed.

In a first section the considered structure is described. The large stadium roof (230x200 meters) is composed of an upper envelope supported by its structural frame. A part of this roof is retractable in order to close the stadium during exhibitions or severe winter conditions. The structural system contains two pre-stressed statically determined main beams (205 meters span length) and two secondary beams (80 meters span length). Characteristics of the 3D finite element model and results of the modal analysis have been provided by the design team. Internal forces in twelve specific elements of the frame are studied using the aerodynamic loading measured in the wind tunnel. The post-processing of the measured data starts by separating the mean and the fluctuating part of the pressures; further, PSD of the fluctuating part are computed. By these processing, some shortcomings of typical measurement signals are identified.

Finally, conclusions of this study are made and negative and positive aspects of the different methods applied are analysed. Also, prospects for advanced studies are given.

## 2 STUDIED STRUCTURE: "LE GRAND STADE DE LILLE MÉTROPOLE"

### *2.1 Description*

The structure studied in this paper is the roof of the stadium *Le Grand Stade de Lille Métropole* currently under construction in Lille, France. Its specificities are a retractable roof and a moving half-playing field. Its dimensions are 230x200x36 meters. The roof is made up of three parts: above the grandstands, above the ambulatories and above the playground as shown in Figure 1.

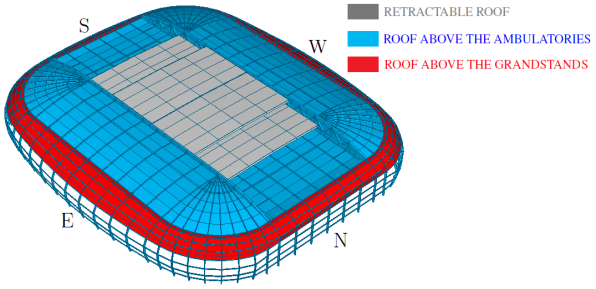


Figure 1. Different parts of the roof, and model of the stadium (N, S, E and W indicate the North, South, East and West, respectively).

Figure 2 shows a view inside the stadium from East to West.

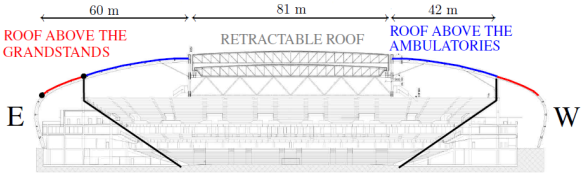


Figure 2. Cross-section from East to West with transversal dimensions.

As shown in Figures 1 and 2 the retractable roof is composed of four elements; the two innermost ones are above the other two, in order to allow their motion. The retractable roof slides on eccentric beams connected to the middle of the main beams (depicted in red in Figure 3(a)). These main beams are statically determined and span 205 meters. They are actually 15 meter high truss beams. Consequently to this large span, the main beams are pre-stressed. Secondary beams (depicted in red in Figure 3(b)) are connected to the main beams and are also truss beams (8 meter high, spanning 80 meters). Figure 4 depicts the different components of the structural system bearing the weight of the roof above the grandstands and the ambulatories. Foremost, the weight of the retractable roof is transmitted via purlins which are perpendicularly fixed to the lower and upper beams which compose the supporting structure (shown in red in Figure 4,(a,b,c)). The weight of the roof above grandstands oriented East and West is borne by fifty-two upper beams. These beams are statically determined and transversally spaced by 13,44 m. On a side they lean on the main beams and on the other side on the metallic supports (shown in red in Figure 4(d)). Supports transmit the loads on the top of the concrete grandstands.

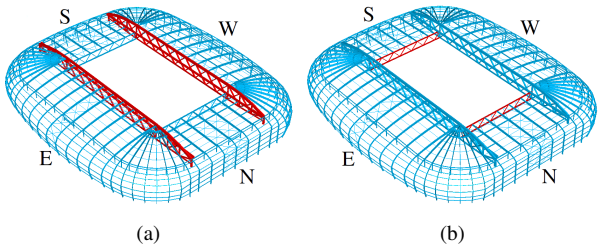


Figure 3. Localisation of the main and secondary beams in the structure: (a) main beams, (b) secondary beams.

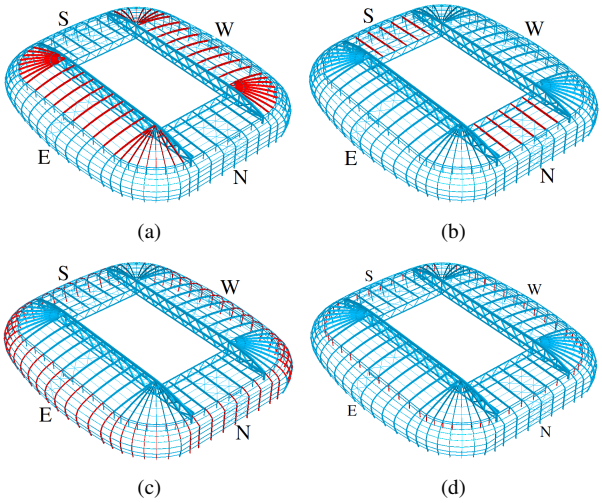


Figure 4. (a) Upper beams east and west, (b) Upper beams north and south, (c) Lower beams, (d) Supports.

For grandstands oriented North and South, upper beams (shown in red in Figure 4(b)) lean on one side on secondary beams and the other side on the metallic supports. The roof above the ambulatories is realized by sixty-six lower beams shown in red in Figure 4(c). On the upper extremity they lean on the metallic supports and at the lower extremity they are connected to the concrete structure on the ground.

### *2.2 Finite element model*

The finite element model has been realised with FinelG (a FE software developed at the University of Liège since 1978 [4]) by the design office Greisch [5]. Table 1 collects principal characteristics of the 3D finite element model for the studied structure.

Table 1. Characteristics of the 3D finite element model.

| | |
|---|---|
| Number of elements | 4940 |
| Number of types of elements | 11 |
| Types of material | 3 |
| Number of geometries | 153 |
| Number of degrees of freedom | 42006 |

### *2.3 Modal properties of the roof structure*

The frequency of the first mode is equal to 0.475 Hz and eleven vibration modes have a natural frequency lower than 1 Hertz.

The design office has decided to keep the first twenty-one modes for the modal analysis which corresponds to a frequency range lower than 1.415 Hz. Figure 5(a) depicts the fundamental mode which is an antisymmetric vertical one and Figure 5(b) depicts the third mode which represents a general vertical movement. A modal damping ($\xi$) equal to 1% for each mode is considered.

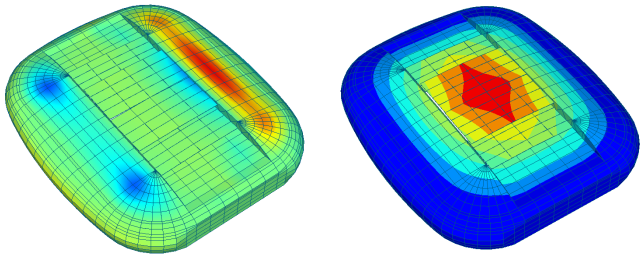

(a) Mode 1: 0.475 Hz. (b) Mode 3: 0.517 Hz.

Figure 5. Modal vertical displacements and associated frequencies.

### 2.4 *Studied elements*

A dedicated focus is put on the ultimate goal of designing the structure, i.e. of estimating extreme values of internal forces. Twelve elements have been selected for this part of the study and are identified in Figure 6.

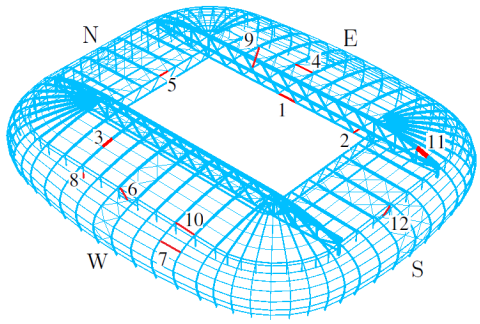


Figure 6. Localisation of the twelve elements in the structure.

Table 2 gives the description of the studied elements for an easy identification into the structure. Only one internal force is studied by element: $N$ corresponds to an axial force and $M_y$ to a bending moment in the vertical plane.

## 3 WIND TUNNEL SIMULATION

### 3.1 *Simulated wind properties*

The target wind properties are based on the Eurocode EN 1991-1-4 [6] and its french national appendix [7]. A IIIa category terrain is appropriate to represent the surrounding of the stadium. Table 3 presents the main parameters of this characterisation. The loads induced by these wind properties correspond to the Service Limit State ones.

### 3.2 *Wind tunnel measurements*

Wind tunnel measurements have been carried out at the *Centre Scientifique et Technique du Bâtiment* in Nantes in France. Figure 7 shows the 1/200 scaled model in the wind tunnel. The surrounding buildings and trees are modelled in the wind tunnel to simulate the environment of the stadium. Instrumentation of the scaled model needed approximately five hundred synchronous pressure sensors. The scaled model is supposed to be infinitely rigid. The sampling frequency 200 Hz corresponds to 2.94 Hz in full scale; so the Nyquist frequency is equal to 1.47 Hz and the time step is equal to 0.342 seconds. Each measurement lasts about 105 minutes full scale. Twenty four wind directions (0° to 345° with a step of 15°) have been tested for ten configurations of the retractable roof. This paper considers only one configuration, 75° wind direction (wind acting perpendicular to the longitudinal East side), retractable roof 100% closed (depicted in Figure 9).

Table 2. List of the studied elements, with considered internal force.

| N° | Description | |
|---|---|---|
| 1 | Lower fiber of the main beam | $N$ |
| 2 | Diagonal of the main beam | $N$ |
| 3 | Element of the upper beam | $M_y$ |
| 4 | Metallic purlin of the roof | $N$ |
| 5 | Upper fiber of the secondary beam | $N$ |
| 6 | Bracing | $N$ |
| 7 | Lower purlin of the roof | $N$ |
| 8 | Metallic support | $N$ |
| 9 | Bracing | $N$ |
| 10 | Peripheral purlin of the roof | $N$ |
| 11 | Upper fiber of the main beam | $N$ |
| 12 | Bracing between support and an upper beam | $N$ |

Table 3. Target wind properties.

| | |
|---|---|
| **Fundamental wind velocity** | |
| Basic wind velocity | $V_{b,0}$=26 m/s |
| Directional factor | $C_{dir}$=1 |
| Seasonal factor | $C_{season}$=1 |
| Return period | 50 years |
| Basic wind velocity | $V_b$=26 m/s |
| **Mean Wind** | |
| Terrain category 3a | $Z_0 = 0,2$ m, $Z_{min} = 5$ m |
| Height of the structure | $Z_s = 36,43$ m |
| Roughness factor | $k_r = 0,209$, $c_r(Z_s) = 1,09$ |
| Orography factor | $c_0 = 1$ |
| Mean wind | $V_m(Z_s) = 28,3$ m/s |
| **Wind Turbulence** | |
| Turbulence factor | $k_1 = 1$ |
| Turbulence Intensity | $I_v(Z_s) = 19\%$ |
| **Peak velocity pressure** | |
| Reference velocity pressure | $q_{mean}(z_s) = 491,7$ N/m$^2$ |
| Peak factor | $g = 3,5$ |
| Peak velocity pressure | $q_p(z_s) = 1133$ N/m$^2$ |

### 3.3 *Post processing of the measured pressures*

As a first step, wind loads can be separated as a sum of two parts:

$$\mathbf{p}(t) = \mu_{\mathbf{p}} + \mathbf{p_0}(t) \quad (1)$$

Figure 7. Model of the stadium in the wind tunnel.

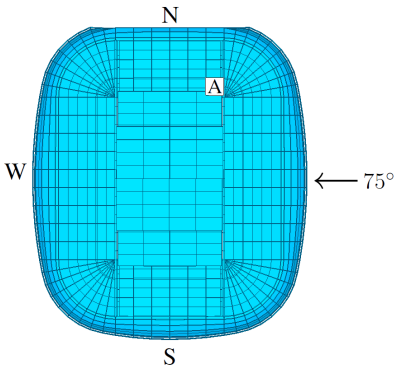


Figure 8. Only wind direction studied in this paper.

where $\mu_{\mathbf{p}}$ and $\mathbf{p_0}(t)$ are the mean and the fluctuation part of wind loads, respectively. An analysis of maps of the means and standard deviations of the pressures reveals a typical pattern and is therefore not illustrated here. Further, an interesting insight into the acquired data consists in analysing the PSD's of the fluctuation part of the measured pressures. PSD's are computed using Welch's method with a Hamming window. This operation reveals a typical decreasing PSD (see Figure 10 for sensor A located in the NE part of the roof, see Figure 8). It appears that almost all acquired pressures are noised by significant harmonic oscillations (they are labelled and pointed with dots in Figure 10). Several reasons can explain these spurious harmonic frequencies: aliased rotation speed of flans, AC power insufficiently filtered, flexibility of the scale model, flexibility of the turning table, etc.

## 4 STRUCTURAL DESIGN FROM WIND TUNNEL MEASUREMENTS

Let us consider $\mathbf{z}(t)$ a set of structural *responses* of interest. Symbol $\mathbf{z}$ may therefore refer to nodal displacements ($\mathbf{z} \equiv \mathbf{x}$), modal displacements ($\mathbf{z} \equiv \mathbf{q}$), internal forces ($\mathbf{z} \equiv \mathbf{f}$), etc or any combination of them.

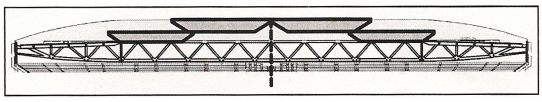

Figure 9. Considered configuration: 100 % Closed.

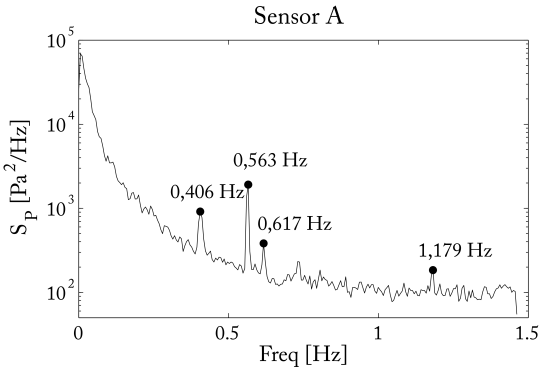


Figure 10. PSD of measured pressure. The number of points is 512 (total number of points is equal to 18432) with an overlap of 50%.

It is divided into three contributions:

$$\mathbf{z}(t) = \mu_{\mathbf{z}} + \underbrace{\mathbf{z_B}(t) + \mathbf{z_R}(t)}_{\mathbf{z_D}(t)} \tag{2}$$

where $\mu_{\mathbf{z}}$, $\mathbf{z_B}(t)$, $\mathbf{z_R}(t)$ and $\mathbf{z_D}(t)$ are the mean, background, resonant and dynamic contributions of responses, respectively.

### 4.1 *Calculation of the mean and background contribution of the responses*

The calculation of $\mu_{\mathbf{z}}$ and $\mathbf{z_B}(t)$ is done in the nodal basis which is more appropriate. For these contributions, a static linear analysis is performed:

$$\mu_{\mathbf{z}} = \mathbf{A}\mu_{\mathbf{p}} \tag{3}$$

$$\mathbf{z_B}(t) = \mathbf{A}\mathbf{p_0}(t) \tag{4}$$

where $\mathbf{A}$ is a matrix of influence coefficients obtained from the stiffness matrix $\mathbf{K}$, in a FE context.

### 4.2 *Calculation of the resonant contribution of the responses*

The dynamic calculation is performed efficiently in the modal basis so that the damping matrix is diagonal and the equations of motion are uncoupled. Only the fluctuation part of wind loads, $\mathbf{p_0}(t)$, is now considered. A special attention has to be paid to the fact that the background component has already been accounted for in the nodal basis. Only the the estimation of the resonant contribution remains to be assessed. Depending on the method of analysis, different approaches are considered next to separate the background component. However, a common stage of the different methods presented hereinafter is the computation of the generalized forces $\mathbf{p_0^\star}(t)$, which is (deterministically) performed in the time domain, by projection of the measured pressures into the known mode shapes $\phi$:

$$\mathbf{p_0^\star}(t) = \phi^{\mathbf{T}}\mathbf{p_0}(t) \tag{5}$$

Mode shapes are also obtained with the FE model. Let $\mathbf{q}(t)$ be the modal responses under $\mathbf{p_0^\star}(t)$. They are computed next with three different approaches.

1. Deterministic time domain:
The modal displacements $\mathbf{q}(t)$ are the solution of the equations of motion:

$$\mathbf{M}^\star \ddot{\mathbf{q}}(t) + \mathbf{C}^\star \dot{\mathbf{q}}(t) + \mathbf{K}^\star \mathbf{q}(t) = \mathbf{p}_0^\star(t) \tag{6}$$

where $\mathbf{M}^\star$, $\mathbf{C}^\star$ and $\mathbf{K}^\star$ are respectively the generalized mass, damping and stiffness matrices (known from the FE model) and the dot denotes time derivative. Newmark's algorithm [10] ($\alpha = 0.25$ and $\delta = 0.5$) is used to solve (6). The background contribution of the modal displacements is given by:

$$\mathbf{q}_\mathbf{B}(t) = \mathbf{K}^{\star^{-1}} \mathbf{p}_0^\star(t) \tag{7}$$

so that the resonant contribution of the modal displacements is here obtained by a simple subtraction:

$$\mathbf{q}_\mathbf{R}(t) = \mathbf{q}(t) - \mathbf{q}_\mathbf{B}(t) \tag{8}$$

and the resonant contribution of the responses is calculated using:

$$\mathbf{z}_\mathbf{R}(t) = \phi^{(\mathbf{z})} \mathbf{q}_\mathbf{R}(t) \tag{9}$$

where $\phi^{(\mathbf{z})}$ is a modal matrix of influence coefficients (obtained from a FE model too).
2. Deterministic frequency domain:
The modal transfer function is modified by subtraction of its value at the origin. This transformation leads to a *resonant modal transfer function*, $\mathbf{H}_\mathbf{R}^\star(\omega)$, defined by:

$$\mathbf{H}_\mathbf{R}^\star(\omega) = \mathbf{H}^\star(\omega) - \mathbf{K}^{\star^{-1}} \tag{10}$$

which allows to calculate the Fourier Transform of the resonant contribution of the modal displacements by solving the equation:

$$\mathbf{Q}_\mathbf{R}(\omega) = \mathbf{H}_\mathbf{R}^\star(\omega) \mathbf{P}_\mathbf{0}^\star(\omega) \tag{11}$$

where $\mathbf{Q}_\mathbf{R}(\omega)$ is the Fourier transform of $\mathbf{q}_\mathbf{R}(t)$; $\mathbf{H}_\mathbf{R}^\star(\omega)$ is the resonant modal transfer function and $\mathbf{P}_\mathbf{0}^\star(\omega)$ is the Fourier transform of $\mathbf{p}_\mathbf{0}^\star(t)$. The resonant contribution of the modal displacements is then calculated using the inverse Fourier transform:

$$\mathbf{q}_\mathbf{R}(t) = \int_{-\infty}^{+\infty} \mathbf{Q}_\mathbf{R}(\omega) e^{j\omega t} d\omega \tag{12}$$

and the resonant contribution of the responses, $\mathbf{z}_\mathbf{R}(t)$, is obtained with (9), as done before in the time domain.
3. Stochastic frequency domain: In a stochastic context, the background resonant decomposition (B/R) is usual in the design of large structures [8]. Indeed, calculation and storage of the spectral densities of the responses of the structure (i.e. nodal/modal displacements, inner forces, etc) are time/memory consuming and therefore usually not performed. Because it is more appropriate, the calculation is here performed in the nodal basis for the background component and in the modal basis for the resonant one. The PSD matrix of the modal coordinates, $\mathbf{S}^{(\mathbf{q})}(\omega)$, is obtained as:

$$\mathbf{S}^{(\mathbf{q})}(\omega) = \mathbf{H}^\star(\omega) \mathbf{S}^{(\mathbf{p}_0^\star)}(\omega) \overline{\mathbf{H}^\star(\omega)^\mathbf{T}} \tag{13}$$

where $\mathbf{S}^{(\mathbf{p}_0^\star)}(\omega)$ is the PSD matrix of the generalized forces (obtained as explained next). Using the well-known B/R decomposition, $\mathbf{S}^{(\mathbf{q})}(\omega)$ can be dispatched into two contributions:

$$\mathbf{S}^{(\mathbf{q})}(\omega) = \underbrace{\mathbf{K}^{\star^{-1}} \mathbf{S}^{(\mathbf{p}_0^\star)}(\omega) \mathbf{K}^{\star^{-\mathbf{T}}}}_{\mathbf{S}^{(\mathbf{q_B})}(\omega)} + \underbrace{\mathbf{H}^\star(\omega) \mathbf{S}_\mathbf{wn}^{(\mathbf{p}_0^\star)} \overline{\mathbf{H}^\star(\omega)^\mathbf{T}}}_{\mathbf{S}^{(\mathbf{q_R})}(\omega)} \tag{14}$$

where $\mathbf{S}_\mathbf{wn}^{(\mathbf{p}_0^\star)}$ is the equivalent white noise matrix of the generalized forces; $\mathbf{S}^{(\mathbf{q_B})}(\omega)$ is the PSD matrix of the background contribution of the modal coordinates and $\mathbf{S}^{(\mathbf{q_R})}(\omega)$ is the PSD matrix of the resonant contribution of the modal coordinates. The introduction of a full white noise matrix instead of just a diagonal matrix allows the treatment in a CQC context in place of SRSS as usual. This method is detailed in [3]. Only its formulation is given here:

$$\mathbf{S}_\mathbf{wn}^{(\mathbf{p}_0^\star)} = \begin{cases} S_m^{(p_0^\star)}(\omega_m) & \text{for diagonal elements} \\ \overline{\Gamma_{mn}} \sqrt{S_m^{(p_0^\star)}(\omega_m) S_n^{(p_0^\star)}(\omega_n)} & \text{for off-diagonal elements} \end{cases} \tag{15}$$

where $S_m^{(p_0^\star)}(\omega_m)$ is the value of the auto PSD of the mth generalized force at its natural frequency $\omega_m$. An appropriate choice of $\overline{\Gamma_{mn}}$ is:

$$\overline{\Gamma_{mn}} = \frac{\Gamma_{mn}(\omega_m) + \Gamma_{mn}(\omega_n)}{2} \tag{16}$$

where $\Gamma_{mn}(\omega)$ is the coherence function between the mth and nth generalized forces defined by:

$$\Gamma_{mn}(\omega) = \frac{S_{mn}^{(p_0^\star)}(\omega)}{\sqrt{S_m^{(p_0^\star)}(\omega) S_n^{(p_0^\star)}(\omega)}} \tag{17}$$

where $S_{mn}^{(p_0^\star)}(\omega)$ is the cross PSD between mth and nth generalized forces.
Finally, the PSD matrix of the resonant contribution of the responses is computed using:

$$\mathbf{S}^{(\mathbf{z_R})}(\omega) = \phi^{(\mathbf{z})} \mathbf{S}^{(\mathbf{q_R})}(\omega) \overline{\phi^{(\mathbf{z})}}^\mathbf{T} \tag{18}$$

Actually [3] proposes an estimation of the correlation coefficient of the modal displacements as :

$$\rho_{mn}^{(q)} \simeq \gamma_B \, \rho_{mn}^{(q_B)} + \gamma_R \, \rho_{mn}^{(q_R)} \tag{19}$$

where $\rho_{mn}^{(q_B)}$ and $\rho_{mn}^{(q_R)}$ are modal correlation coefficients that would be obtained in case of perfectly background (resp. resonant) responses. The weighting coefficients $\gamma_B$ and $\gamma_R$ result from a solid mathematical development [3] and aim at providing an accurate estimation of $\rho_{mn}^{(q)}$ in case of mixed response.

### *4.3 Computation of extreme values*

A counting procedure in the time domain is applied in the deterministic approaches. Both deterministic methods provide the resonant contribution of the responses in the time domain, eventually after ifft (Inverse Fast Fourier Transform). The

background contribution calculated in the nodal basis, see (4), added up to the resonant contribution calculated in the modal basis, see (9), gives the dynamic contribution of the responses:

$$\mathbf{z_D}(t) = \underbrace{\mathbf{z_B}(t)}_{\text{from a nodal analysis}} + \underbrace{\mathbf{z_R}(t)}_{\text{from a modal analysis}} \tag{20}$$

This is precisely the extremum of $\mathbf{z_D}(t)$ that has to be determined. This is performed with a three-step procedure:

1. each record is virtually divided into twelve sub-records of about 10 minutes each [6] and the extreme values (min and max) of each one are identified:

$$\mathbf{z}_{\mathbf{D,i}}^{(\mathbf{min})} = min\ \mathbf{z}_{\mathbf{D,i}}(t);\ \ \mathbf{z}_{\mathbf{D,i}}^{(\mathbf{max})} = max\ \mathbf{z}_{\mathbf{D,i}}(t)\ \ for\ i=1,2,...12 \tag{21}$$

2. these maxima and minima are averaged to obtain the expected maximum and minimum, over the 10-min. observation period:

$$\mathbf{z}_{\mathbf{D}}^{(\mathbf{emin})} = \frac{\sum_{i=1}^{12}\mathbf{z}_{\mathbf{V,i}}^{(\mathbf{min})}}{12};\ \ \mathbf{z}_{\mathbf{D}}^{(\mathbf{emax})} = \frac{\sum_{i=1}^{12}\mathbf{z}_{\mathbf{V,i}}^{(\mathbf{max})}}{12} \tag{22}$$

3. positive and negative peak factors are obtained by dividing these expected maximum and minimum by their standard deviations. For the k$^{th}$ response:

$$g_k^- = \frac{z_{D,k}^{(emin)}}{\sigma_{z_{D,k}}};\ \ g_k^+ = \frac{z_{D,k}^{(emax)}}{\sigma_{z_{D,k}}} \tag{23}$$

where $\sigma_{z_{D,k}}$ is the standard deviation of the kth response.

In the stochastic context, another approach to calculate the extreme values is used:

$$z_{D,k}^{(extr)} \simeq \left(\sqrt{2\ln n_0^+} + \frac{\gamma}{\sqrt{2\ln n_0^+}}\right)\sigma_{z_{D,k}} = g\,\sigma_{z_{D,k}} \tag{24}$$

where $\gamma = 0.5772$ is Euler's constant, g is the peak factor (known as Rice's formula [11]), $n_0^+$ is the number of zero up-crossings during the observation period with the following formulation:

$$n_0^+ = \frac{T}{2\pi}\sqrt{\frac{m_k^{2,(z_D)}}{\sigma_{z_{D,k}}}} = \frac{T}{2\pi}\sqrt{\frac{m_k^{2,(z_D)}}{m_k^{0,(z_D)}}} \tag{25}$$

where $T$ is the observation period on the sub-records and $m_k^{2,(z_D)}$ is the auto spectral moment of order 2 of the dynamic contribution of the kth response. More details about its computation are given now. A matrix of spectral moments is defined by:

$$\mathbf{m^i} = \int_{-\infty}^{+\infty} |\omega|^{\mathbf{i}}\mathbf{S}(\omega)\mathbf{d}\omega \tag{26}$$

Application of (26) to (18) provides the spectral moment matrix of the resonant contribution of the responses:

$$\begin{aligned}\mathbf{m}^{\mathbf{i},(\mathbf{z_R})} &= \int_{-\infty}^{+\infty} |\omega|^{\mathbf{i}}\mathbf{S}^{(\mathbf{z_R})}(\omega)\mathbf{d}\omega \\ &= \boldsymbol{\phi}^{(\mathbf{z})}\int_{-\infty}^{+\infty} |\omega|^{\mathbf{i}}\mathbf{S}^{(\mathbf{q_R})}(\omega)\mathbf{d}\omega\ \ \overline{\boldsymbol{\phi}^{(\mathbf{z})}}^{\mathbf{T}} \\ &= \boldsymbol{\phi}^{(\mathbf{z})}\mathbf{m}^{\mathbf{i},(\mathbf{q_R})}\overline{\boldsymbol{\phi}^{(\mathbf{z})}}^{\mathbf{T}}\end{aligned} \tag{27}$$

where $\mathbf{m}^{\mathbf{i},(\mathbf{q_R})}$ is the spectral moments matrix of the resonant contribution of the modal displacements. Only the diagonal of $\mathbf{m}^{\mathbf{i},(\mathbf{z_R})}$ is necessary and these elements are in principle calculated using the complete quadratic combination:

$$m_k^{i,(z_R)} = \sum_{m=1}^{M}\sum_{n=1}^{M}\phi_{km}^{(z)}\,\phi_{kn}^{(z)}\,m_{mn}^{i,(q_R)} \tag{28}$$

where $M$ is the number of modes. The PSD of $\mathbf{z_B}(t)$ is calculated via Welch's method from the value obtained in (4) in the nodal basis and the matrix of spectral moments as in (26). Finally:

$$m_k^{i,(z_D)} = \underbrace{m_k^{i,(z_B)}}_{\text{from a nodal analysis}} + \underbrace{m_k^{i,(z_R)}}_{\text{from a modal analysis}} \tag{29}$$

so that (25) and (24) may be applied.

## 5 FITTING OF A MODEL ONTO THE GENERALIZED FORCES

Section 3.3 has thrown light onto some shortcomings related to the measured signals. Their potential impact on the structural response must be assessed carefully. The influence of noise frequencies on the background contribution is relatively weak (because they do not affect significantly the variance). On the contrary for the resonant contribution, the diagonal elements of the white noise matrix are directly related to the values taken by the PSD at the natural frequencies. So if a deterministic analysis is applied without an appropriate processing of the measured data (which is not a trivial task), it is suggested to check at least that noise frequencies are not too close to with the structural natural frequencies. A proposed criterion is to fix a frequency range around each natural frequency where no noise frequencies can be present. This range can be the half height width of the peak of the transfer function which is equal to $2\xi f_{nat}$. So one of the two following conditions should be validated:

$$f_{noise} > (1+\xi)f_{nat}\ \text{ or }\ f_{noise} < (1-\xi)f_{nat} \tag{30}$$

where $f_{noise}$, $\xi$ and $f_{nat}$ are the frequency of the noise, the damping ratio and the natural frequency, respectively. For this study, this criterion has been checked and validated as shown at Figure 11.

As developed in section 4.2, the calculation of the equivalent white noise matrix, $\mathbf{S}_{\mathbf{wn}}^{\mathbf{p_0^\star}}$, requires estimation of the PSD matrix of the generalized forces, $\mathbf{S}^{(\mathbf{p_0^\star})}(\boldsymbol{\omega})$, for every natural frequency. The analysis method proposed in this paper precisely consists in fitting a probabilistic model onto the deterministic generalized forces $\mathbf{p_0^\star(t)}$. In a stochastic approach a possible solution is to follow this four-step method:

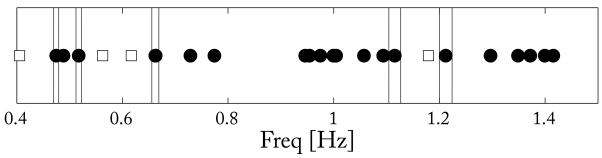


Figure 11. Squares represent the noise frequencies and dots represent the natural frequencies. In potentially critical cases vertical lines represent the range around the natural frequencies where no noise frequencies are allowed to be present.

1. calculation of the PSD via Welch's method (or another classical method);
2. identification of the noise frequencies (a criterion has to be adopted, more details can be found in [9]);
3. filtering of the noise frequencies by a band-stop;
4. calculation of the PSD on the filtered signal with a parametric estimator ($6^{th}$ order Yule-Walker).

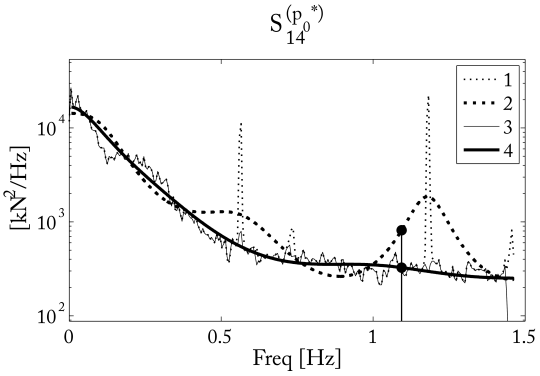


Figure 12. Application of the proposed solution. 1=Welch's method - raw signal; 2=Yule-Walker - raw signal; 3=Welch's method - filtered signal and 4=Yule-Walker - filtered signal. Dots have an abscissa equal to the natural frequency of the mode.

This solution restores the energy for filtered noise frequencies. Figure 12 shows the effectiveness of the proposed solution for the auto PSD of the generalized force in the 14th mode. Indeed it gives good results as the curve 4 smoothly represents the actual signal without being affected by the noise frequencies. Moreover curve 2 shows that the application of a parametric method onto noised generalized forces is not recommended. In fact the value taken at the natural frequency (dot on curve 2) is erroneous. As a conclusion, the stochastic approach is a smart way to bypass the drawbacks related to these noise frequencies. Indeed, a stochastic model is fitted on the generalized forces, for the whole frequency range, independent of the noise frequencies. In addition to providing a simple way to treat these noise frequencies, it also provides a model that is consistent with physical intuition.

## 6 RESULTS

### *6.1 Modal coordinates*

As a first comparison, PSD of the modal coordinates obtained with the three analysis methods are given in Figure 13.

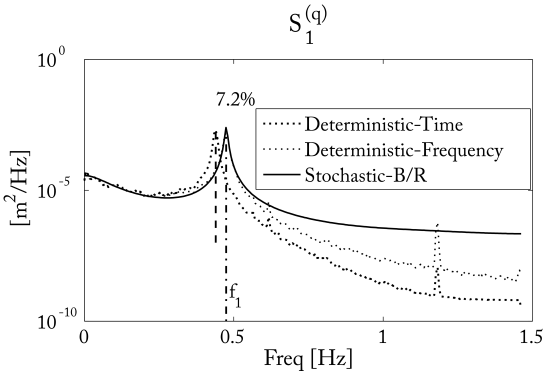


Figure 13. PSD of the first modal coordinate for the three analysis methods. The vertical dash-dotted line indicates the natural frequency. The vertical dashed line represents the frequency corresponding to the peak obtained with the Deterministic-Time domain method.

Owing to the typical smallness of the sampling frequency, results show that the deterministic step-by-step method produces period elongation [10] and is therefore not recommended. The deterministic Fourier transform and the stochastic approach yield very similar results. However, the advantage of a stochastic-B/R decomposition is that it does not take into account noise frequencies and the results depend on a probabilistic property fitted on the measured data. The results from the deterministic approach still show noise frequencies; they also depend on a unique non repeatable measurement (all other things remaining equal) and the PSD's have an erratic behaviour. As an illustration, Figure 14 presents the modal correlation coefficient $\rho_{mn}^{qB}$ (upper left corner) related to the background contribution that would be obtained in a modal analysis. If the dynamic behaviour was essentially quasi-static, it would reflect the actual correlation pattern between modal responses. However, it results from a weighting with the resonant component $\rho_{mn}^{qR}$ (lower right corner) so that for this particular structure and loading, the resulting correlation matrix is fairly diagonal, see Figure 15, which shows a predominant resonant behaviour. This further indicates that SRSS is probably acceptable for this problem.

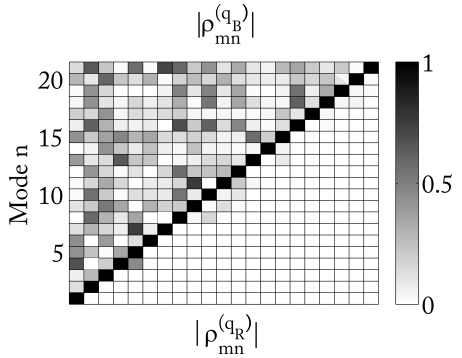


Figure 14. Correlation coefficient of the background (upper left corner) and the resonant (lower right corner) contribution of $q$.

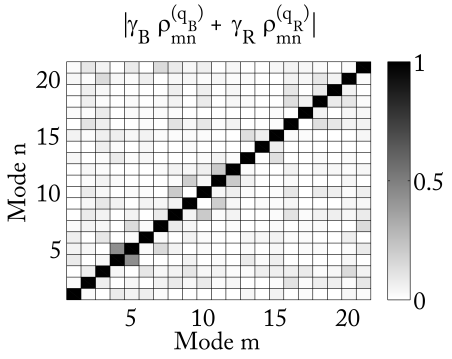


Figure 15. Dynamic correlation coefficient of $q$.

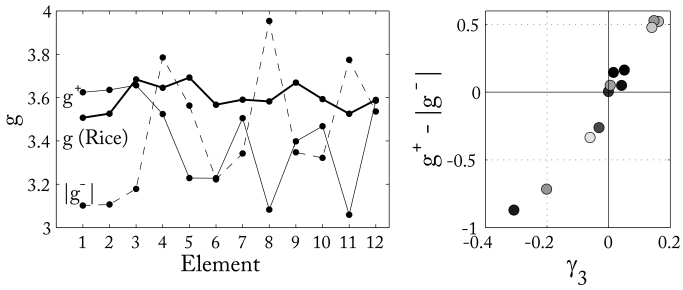


Figure 16. The peak factors obtained from the deterministic and the stochastic approach (left). The correlation between $g^+ - |g^-|$ and the skewness coefficient $\gamma_3$ (right) (calculated via the Deterministic - Frequency approach).

### *6.2 Evaluation of extreme values*

Extreme values are computed for twelve elements of the roof's structure. Table 4 collects standard deviations obtained with the deterministic - frequency approach (second row) and the stochastic approach (third row). They show a very good agreement. Peak factors from the two methods are represented in Figure 16. The deterministic counting process is able to capture the non Gaussian nature of the loading (henceforth of the response) and provides therefore positive and negative peak factors. This is explained by the skewness of the response (itself due to the skewness of the loading). On the contrary, Rice's formula for extreme values was developed under the assumption of a Gaussian process and provides therefore a unique peak factor. The positive and negative peak factors do not necessarily bracket the peak factor obtained with Rice's formula (e.g. E: 3, 5, 6, 7, 9 and 10). Moreover the difference between the positive and negative peak factors can be important (see E-8).

Table 4. Standard deviations ($\sigma$). Units: kN and kN.m.

| | E1 | 2 | 3 | 4 | 5 | 6 | 7 | 8 | 9 | 10 | 11 | 12 |
|---|---|---|---|---|---|---|---|---|---|---|---|---|
| $\sigma_f$ | 766 | 96 | 100 | 152 | 129 | 77 | 11 | 10 | 37 | 28 | 328 | 82 |
| | 757 | 95 | 95 | 151 | 123 | 74 | 11 | 10 | 36 | 28 | 321 | 82 |

Figure 16 also plots $g^+ - |g^-|$ versus the skewness coefficient $\gamma_3$. The correlation between the difference in peak factors and the skewness coefficients is strong and positive: a positive skewness coefficient corresponds to a positive peak factor greater than the negative one and vice versa.

## 7 CONCLUSIONS

The use of a stochastic approach from deterministic wind tunnel measurements is benchmarked against a fully deterministic approach. The main argument is obviously the flexibility in pre-processing the time histories measured in the wind tunnel in order to smoothen them. It also provides a model consistent with physical intuition. This study also reveals the need for advanced techniques as presented in [12,13] for suitable estimations of the peak factors in the context of a stochastic approach. Actually, subsequent researches are focused on extending the idea of probabilistic model fitting at the bi-spectrum of the generalized forces [14,15] to perform non-Gaussian analyses for structures under wind loads and to apply extended B/R decomposition to the third order [16].

## ACKNOWLEDGEMENTS

We would like to acknowledge the "Centre Scientifique et Technique du Bâtiment" in Nantes (France) and also the design office "Greisch" in Liège (Belgium) for having provided the measurements in wind tunnels which was the matter of this work.

## REFERENCES

[1] R. W. Clough, J. Penzien, *Dynamics of structures*, Mc Graw-Hill : Civil Engineering series (second edition), 1997.
[2] A. Preumont, *Random Vibration and Spectral Analysis*, Presses polytechniques et universitaires romandes, 1990.
[3] V. Denoël, *Estimation of modal correlation coefficients from background and resonant responses*, Structural Engineering and Mechanics, 32-6, 725-740, 2009.
[4] FinelG, *User's manual, Version 8.2*, Département M&S (Ulg) - Bureau d'Etudes Greisch, 1999.
[5] *http://www.greisch.com*
[6] *Eurocode 1: Actions sur les structures - Partie 1-4: Actions générales - Actions du vent*, Comité Européen de normalisation, Réf. n° EN 1991-1-4:2005 F.
[7] *Eurocode 1: Actions sur les structures - Partie 1-4: Actions générales - Actions du vent, Annexes A à F*, Comité Européen de normalisation, Réf. n° NF EN 1991-1-4:2005/NA.
[8] M. Ashraf Ali, P. L. Gould, *On the resonant component of the response of single degree-of-freedom systems under random loading*, Engineering Structures, 7-4, 280-282, 1985.
[9] N. Blaise, *Étude du comportement d'une toiture de grandes dimensions soumise à un vent turbulent. Application: le Grand Stade de Lille Métropole*, Travail présenté en vue de l'obtention du grade d'Ingénieur civil construction à finalité approfondie, Faculté des Sciences Appliquées, Université de Liège, 2010.
[10] N.M. Newmark, E. Rosenblueth, *Fundamentals of Earthquake Engineering (Civil engineering and engineering mechanics series)*, Prentice-Hall in Englewood Cliffs, N.J, 1971.
[11] S.O. Rice, *Mathematical Analysis of Random Noise*, Bell System Tech. J., 23, 282-332; 24, 45-156, 1945.
[12] C. Floris, L. De Iseppi, *The Peak Factor for Gust Loading: A Review and Some New Proposals*, Meccanica, 33-3, 319-330, 1998.
[13] K. R. Gurley, M. A. Tognarelli, A. Kareem, *Analysis and simulation tools for wind engineering*, Probabilistic Engineering Mechanics, 12-1, 9-31, 1997.
[14] V. Denoël, H. Degée, *Non Gaussian Response of Bridges Subjected to Turbulent Wind Effect of the non Linearity of Aerodynamic Coefficients*, ECCM06, 3rd European Conference on Computational Solid and Structural Mechanics, Lisbon, Portugal, 2006.
[15] V. Gusella, A. L. Materazzi, *Non-Gaussian response of MDOF wind-exposed structures: Analysis by bicorrelation function and bispectrum*, Meccanica, 33-3, 299-307, 1998.
[16] V. Denoël, *On the Background and Biresonant Components of the Random Response of Single Degree-Of- Freedom Systems under non-Gaussian Random Loading*, to appear in Structural Engineering.